Multi-component optical solitary waves

Yuri S. Kivshar[1], Andrey A. Sukhorukov[1], Elena A. Ostrovskaya[1], Tristram J. Alexander[1], Ole Bang[1,2],
Solomon M. Saltiel[3], Carl Balslev Clausen[2], and Peter L. Christiansen[2]

[1] *Optical Sciences Centre, Australian National University, Canberra ACT 0200, Australia*
[2] *Department of Mathematical Modeling, Technical University of Denmark, Lyngby DK-2800, Denmark*
[3] *Quantum Electronics Department, Faculty of Physics, University of Sofia, Sofia 1164, Bulgaria*

We discuss several novel types of multi-component (temporal and spatial) envelope solitary waves that appear in fiber and waveguide nonlinear optics. In particular, we describe multi-channel solitary waves in bit-parallel-wavelength fiber transmission systems for high performance computer networks, multi-colour parametric spatial solitary waves due to cascaded nonlinearities of quadratic materials, and quasiperiodic envelope solitons due to quasi-phase-matching in Fibonacci optical superlattices.

I. INTRODUCTION

Rapid progress in the design and manufacture of optical fiber systems is a result of worldwide demand for ultra-high bit-rate optical communications. This explains the growing interest of the soliton community in soliton-based optical fiber communication systems. This area of research was considerably advanced in recent years [1]. The most remarkable results include the application of the concept of the dispersion management to *temporal optical solitons* and soliton-based optical transmission systems, and the discovery of the so-called *dispersion managed soliton*. High-speed optical communications require effective components such as high-performance broadband computer networks that can be developed by employing the concept of the bit-parallel-wavelength (BPW) pulse transmission that offers many of the advantages of both parallel fiber ribbon cable and conventional wavelength-division-multiplexing (WDM) systems [2].

Expanding development in the study of the soliton fiber systems has been observed in parallel with impressive research on their spatial counterparts, optical self-trapped beams or *spatial optical solitons*. One of the key concepts in this field came from the theory of multi-frequency wave mixing and cascaded nonlinearities where a nonlinear phase shift is produced as a result of the parametric wave interaction [3,4]. In all such systems, the nonlinear interaction between the waves of two (or more) frequencies is the major physical effect that can support coupled-mode multi-frequency solitary waves.

The examples of temporal and spatial solitons mentioned above have one common feature: they involve the study of solitary waves in multi-component nonlinear models. The main purpose of this paper is to overview several different physical examples of multi-mode and/or multi-frequency solitary waves that occur for the pulse or beam propagation in nonlinear optical fibers and waveguides. For these purposes, we select three different cases: multi-wavelength solitary waves in bit-parallel-wavelength optical fiber links, multi-colour spatial solitons due to multistep cascading in optical waveguides with quadratic nonlinearities, and quasiperiodic solitons in the Fibonacci superlattices. We believe these examples display both the diversity and richness of the multi-mode soliton systems, and they will allow further progress to be made in the study of nonlinear waves in multi-component nonintegrable physical models.

II. TEMPORAL AND SPATIAL SOLITONS

Because the phenomenon of the long-distance propagation of *temporal optical solitons* in optical fibers [1] is known to a much broader community of researchers in optics and nonlinear physics, first we emphasize *the difference between temporal and spatial solitary waves.* Indeed, for a long time stationary beam propagation in planar waveguides has been considered somewhat similar to the pulse propagation in fibers. This approach is based on the so-called *spatio-temporal analogy* in wave propagation, meaning that the propagation coordinate z is treated as the evolution variable and the spatial beam profile along the transverse direction in waveguides, is similar to the temporal pulse profile in fibers. This analogy is based on a simple notion that both beam evolution and pulse propagation can be described by the cubic nonlinear Schrödinger (NLS) equation.

However, contrary to the widely accepted opinion, there is a crucial difference between temporal and spatial solitons. Indeed, in the case of the nonstationary pulse propagation in fibers, the operation wavelength is usually selected near the zero point of the group-velocity dispersion. This means that the absolute value of the fiber dispersion is small enough to be compensated by a weak nonlinearity such as that produced by the (very weak) Kerr effect in optical fibers which leads to a relative nonlinearity-induced change in the refractive index. Therefore, nonlinearity in such systems is always weak and it should be well modeled by a cubic NLS equation which is known to be integrable by means of the inverse-scattering technique. However, for very short (e.g., fs) pulses the cubic NLS equation describing the long-distance propagation of pulses should be corrected to include additional terms that would account for such effects as higher-order dispersion, Raman scattering, etc. All such corrections can be taken into account with the

help of the perturbation theory [1]. Thus, in fibers nonlinear effects are weak and they become important only when dispersion is small (near the zero-dispersion point) affecting the pulse propagation over large distances (of order of hundreds of meters or even kilometers). The situation changes dramatically when we consider the propagation of multi-wavelength pulses with almost equal group velocities. The corresponding model is described by a nonintegrable and rather complicated system of coupled NLS equations, which we briefly discuss below.

In contrary to the pulse propagation in optical fibers, the physics underlying the stationary beam propagation in planar waveguides and bulk media is different. In this case an optical beam is generated by a continuous wave (CW) source and it is time independent. However, when the beam evolves with the propagation distance z, it diffracts in the transverse spatial directions. Then, a nonlinear change in the refractive index should compensate for the beam spreading caused by diffraction *which is not a small effect.* That is why to observe spatial solitons as self-trapped optical beams, much larger nonlinearities are usually required, and very often such nonlinearities are not of the Kerr type (e.g. they saturate at higher intensities). This leads to the models of generalized nonlinearities with the properties of solitary waves different from those described by the integrable cubic NLS equation. Propagation distances involved in the phenomenon of the beam self-focusing and spatial soliton propagation are of the order of millimeters or centimeters. To achieve such large nonlinearities, one needs to use the optical materials with large nonlinearity-induced refractive index. One of the possible way to overcome this difficulty is to use the so-called *cascaded nonlinearities* of noncentrosymmetric optical materials where nonlinear effects are accumulated due to parametric wave interaction under the condition of the wave phase matching. Such parametric wave-mixing effects generate novel classes of spatial optical solitons where resonant parametric coupling between the envelopes of two (or more) beams of different frequencies supports stable spatially localised waves even in a bulk medium (see details in Ref. [3]). It is this kind of multi-component solitary waves that we discuss below.

III. BIT-PARALLEL-WAVELENGTH SOLITONS

A growing demand for high-speed computer communications requires an effective and inexpensive computer interconnection. One attractive alternative to the conventional WDM systems is BPW single-mode fiber optics links for very high bandwidth computer communications [2]. They differ from the WDM schemes in that no parallel to serial conversion is necessary, and parallel pulses are launched simultaneously on different wavelengths.

When the pulses of different wavelengths are transmitted simultaneously, the cross-phase modulation can produce an interesting *pulse shepherding effect* [5], when a strong ("shepherd") pulse enables the manipulation and control of pulses co-propagating on different wavelengths in a multi-channel optical fiber link.

To describe the simultaneous transmission of N different wavelengths in a nonlinear optical fiber, we follow the standard derivation [6] and obtain a system of N coupled nonlinear Schrödinger (NLS) equations ($0 \leq j \leq N-1$):

$$i\frac{\partial A_j}{\partial z} + iv_{gj}^{-1}\frac{\partial A_j}{\partial t} - \frac{\beta_{2j}}{2}\frac{\partial^2 A_j}{\partial t^2}$$
$$+\chi_j\left(|A_j|^2 + 2\sum_{m \neq j}|A_m|^2\right)A_j = 0, \tag{1}$$

where, for the $j-$th wave, $A_j(z,t)$ is the slowly varying envelope, v_{gj} and β_{2j} are the group velocity and group-velocity dispersion, respectively, and the nonlinear coefficients χ_j characterize the Kerr effect. Equations (1) do not include the fiber loss, since the fiber lengths involved in bit-parallel links are only a small fraction of the attenuation length.

We measure the variables in the units of the central wavelength channel (say, $j = 0$), and obtain the following normalized system of the N coupled NLS equations,

$$i\frac{\partial u_j}{\partial z} + \frac{1}{2}\alpha_j\frac{\partial^2 u_j}{\partial t^2}$$
$$+\gamma_j\left(|u_j|^2 + 2\sum_{m \neq j}|u_m|^2\right)u_j = 0, \tag{2}$$

where $u_j = A_j/\sqrt{P_0}$, P_0 is the incident optical power in the central channel, $\alpha_j \equiv (\beta_{2j}/|\beta_{20}|)$, $\gamma_j \equiv \chi_j/\chi_0$, so that $\alpha_0 = \gamma_0 = 1$. For the operating wavelengths spaced 1 nm apart within the band $1530 \div 1560$ nm, the coefficients α_j and γ_j are different but close to 1. Initially, in Eq. (2), we omit the mode walk-off effect described by the parameters $\delta_j = v_{g0}^{-1} - v_{gj}^{-1}$ (so that $\delta_0 = 0$). This effect will be analysed later in this section.

To analyze the nonlinear modes, i.e. localized states of the BPW model (2), we look for stationary solutions in the form,

$$u_j(z,t) = u_j(t)e^{i\beta_j z}, \tag{3}$$

and therefore obtain the system of equations for the normalized mode amplitudes,

$$\frac{1}{2}\frac{d^2 u_0}{dt^2} + \left(|u_0|^2 + 2\sum_{n=1}^{N-1}|u_n|^2\right)u_0 = \frac{1}{2}u_0,$$
$$\frac{1}{2}\alpha_n\frac{d^2 u_n}{dt^2} + \gamma_n\left(|u_n|^2 + 2\sum_{m \neq n}|u_m|^2\right)u_n = \lambda_n u_n, \tag{4}$$

where $n = 1, 2, \ldots, N-1$, the amplitudes and time are measured in the units of $\sqrt{2\beta_0}$ and $(2\beta_0)^{-1/2}$, respectively, and $\lambda_n = \beta_n/2\beta_0$.

System (4) has *exact analytical solutions* for N coupled components, the so-called *BPW solitons*. Indeed, looking for solutions in the form $u_0(t) = U_0 \; \text{sech}\, t$, $u_n(t) = U_n \; \text{sech}\, t$, we obtain the constraint $\lambda_n = \alpha_n/2$, and a system of N coupled algebraic equations for the wave amplitudes,

$$U_0^2 + 2\sum_{n=1}^{N-1} U_n^2 = 1, \;\; U_n^2 + 2\sum_{m\neq n} U_m^2 = \alpha_n/\gamma_n.$$

In a special symmetric case, we take $\alpha_n = \gamma_n = 1$, and the solution of those equations is simple [7]: $U_0 = U_n \equiv U_* = [1 + 2(N-1)]^{-1/2}$.

Analytical solutions can also be obtained in the *linear limit*, when the central frequency pulse (at $n = 0$) is large. Then, linearizing Eqs. (4) for small $|u_n| \ll |u_0|$, we obtain a decoupled nonlinear equation for u_0 and $N-1$ decoupled linear equations for u_n. Each of the latter possess a localized solution provided $\lambda_n = \lambda_n^{(0)}$, where $\lambda_n^{(0)} = (\alpha_n/8)[1 - \sqrt{1 + 16(\gamma_n/\alpha_n)}]^2$. In this limit the central soliton pulse u_0 ("shepherd pulse") can be considered as inducing an effective waveguide that supports a fundamental mode u_n with the corresponding cutoff $\lambda_n^{(0)}$. Since, by definition, the parameters α_n and γ_n are close to 1, we can verify that the soliton-induced waveguide supports maximum of two modes (fundamental and the first excited one). This is an important physical result that explains the effective robustness of the pulse guidance by the shepherding pulse.
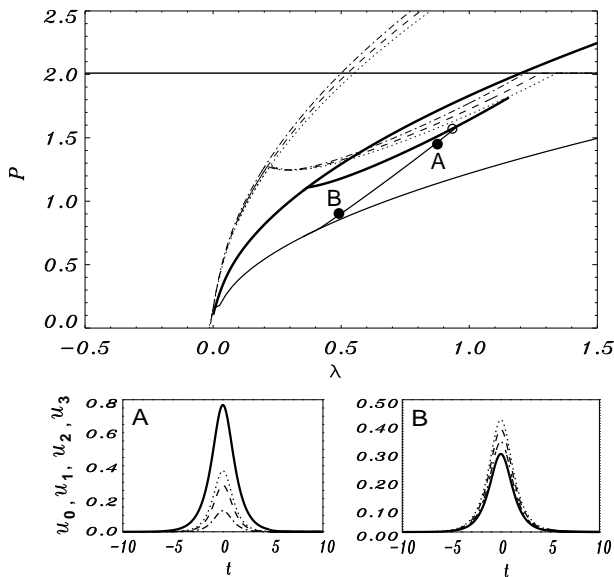

FIG. 1. Bifurcation diagram (top) and two examples of the stationary BPW soliton solutions for $N = 4$.

To demonstrate a number of unique properties of the multi-channel BPW solitons, we consider the case $N = 4$ in more details. A comprehensive discussion of the case $N = 2$ can be found in the preprint [8]. We select the following set of the normalized parameters: $\alpha_{0,3} = \gamma_{0,3} = 1$,

$\alpha_1 = \gamma_1 = 1.1$, and $\alpha_2 = \gamma_2 = 1.05$. Solitary waves of this four-wavelength BPW system can be found numerically as localized solutions of Eqs. (4). Figure 1 presents the lowest-order families of such localized solutions. In general, they are characterized by $N - 1$ parameters, but we can capture the characteristic features by presenting power dependencies along the line $\lambda \equiv \lambda_1 = \lambda_2 = \dots$ in the parameter space $\{\lambda_n\}$. The power of the central-wavelength component ($n = 0$) does not depend on λ (straight line $P_0 = 2$). Thin dashed, dotted, and dash-dotted curves correspond to the three separate single-mode solitons of the multi-channel BPW system, (1), (2), and (3), respectively, shown with the corresponding branches of (0+1), (0+2), and (0+3) two-mode solitons. The latter curves start off from the bifurcation points on the u_0 branch at $\lambda_1^{(0)}$, $\lambda_2^{(0)}$, and $\lambda_3^{(0)}$, respectively. Close separation of those curves is the result of closeness of the parameters α_n and γ_n for $n = 1, 2, 3$.

Thick solid curves in Fig. 1 correspond to the two- (1+2) and three-mode (0+1+2) localized solutions. The latter solutions bifurcate and give birth to four-wavelength solitons (0+1+2+3) (branch A-B). Two examples of such four-wave composite solitons are shown in Fig. 1 (bottom row). The solution B is close to an exact sech-type solution at $\lambda = 0.5$ (described above) for $N = 4$, whereas the solution A is close to that approximately described in the linear limit in the vicinity of a bifurcation point. Importantly, for different values of the parameters (α_n, γ_n), the uppermost bifurcation point for this branch (open circle in Fig. 1) is not predicted by a simple linear theory and, due to the nonlinear mode coupling, it gets shifted from the branch of the central-wavelength soliton (straight line) to a two-mode branch (0+1+2) (thick solid curve).

As a result, if we start on the right end of the horizontal branch and follow the lowest branches of the total power $P(\lambda)$ in Fig. 1, we pass the following sequence of the soliton families and bifurcation points: $(0) \rightarrow (0+1) \rightarrow (0+1+2) \rightarrow (0+1+2+3) \rightarrow (1+2+3) \rightarrow (2+3) \rightarrow (3)$. If the modal parameters are selected closer to each other, the first two links of *the bifurcation cascade* disappear (i.e. the corresponding bifurcation points merge), and the four-mode soliton bifurcates directly from the central-wavelength pulse, as predicted by the linear theory. Note however that the sequence and location of the bifurcation points is a function of the cross-section of the parameter space $\{\lambda_n\}$, and the results presented above correspond to the choice $\lambda = \lambda_1 = \lambda_2 = \dots$.

The qualitative picture of the cascading bifurcations preserves for other values of N. In particular, near the bifurcation point a mixed-mode soliton corresponds to the localized modes guided by the central-wavelength soliton (shepherd) pulse. The existence of such soliton solutions is a key concept of BPW transmission when the data are launched in parallel carrying a desirable set of bits of information, all guided by the shepherd pulse at a selected wavelength.

Effects of the walk-off on the multi-channel BPW solitons seems to be most dangerous for the pulse alignment in the parallel links. For nearly equal soliton components, it was shown long time ago [9] that nonlinearity can provide an effective trapping mechanism to keep the pulses together. For the shepherding effect, the corresponding numerical simulations are presented in Figs. 2(a-d) for the four-channel BPW system. Initially, we launch a composite four-mode soliton as an unperturbed solution A [see Fig. 1] of Eqs. (2), without walk-off and centered at $t = 0$. When this solution evolves along the propagation direction z in the presence of small to moderate relative walk-off ($\delta_n \neq 0$ for $n \neq 0$), its components remain strongly localized and mutually trapped [Fig. 2(a,b)], whereas it loses some energy into radiation for much larger values of the relative mode walk-off [Fig. 2(c,d)].
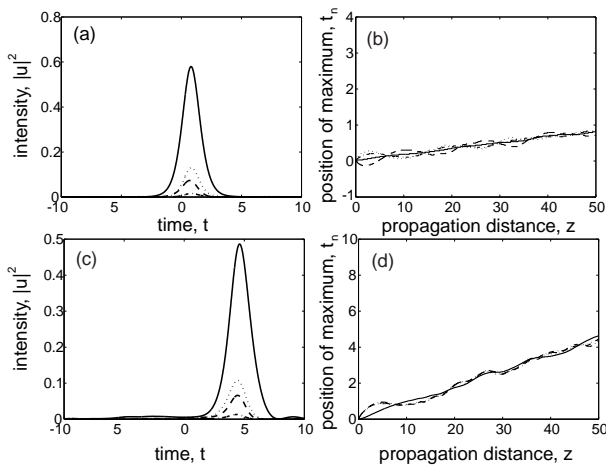

FIG. 2. Influence of the mode walk-off on the shepherding effect for the input pulse A of Fig. 1. Shown are: output pulse at the propagation distance $z = 50$ for (a) $\delta_1 = 0.45, \delta_2 = -0.35, \delta_3 = 0.25$, and (c) $\delta_1 = \delta_2 = \delta_3 = 0.9$; (b,d) — evolution of the position of maximum for all pulse constituents. Solid line — maxima of the shepherd pulse.

IV. PARAMETRIC OPTICAL SOLITONS DUE TO MULTISTEP CASCADING

A. Concept of multistep cascading

Recent progress in the study of cascading effects in optical materials with quadratic (second-order or $\chi^{(2)}$) nonlinear response has offered new opportunities for all-optical processing, optical communications, and optical solitons [3,4]. Most of the studies of cascading effects employ parametric wave mixing processes with a single phase-matching and, as a result, two-step cascading [3]. For example, the two-step cascading associated with type I second-harmonic generation (SHG) includes the generation of the second harmonic ($\omega + \omega = 2\omega$) fol-

lowed by reconstruction of the fundamental wave through the down-conversion frequency mixing (DFM) process ($2\omega - \omega = \omega$). These two processes are governed by one phase-matched interaction and they differ only in the direction of power conversion.

The idea to explore more than one simultaneous nearly phase-matched process, or *double-phase-matched (DPM) wave interaction*, became attractive only recently [10,11], for the purposes of all-optical transistors, enhanced nonlinearity-induced phase shifts, and polarization switching. In particular, it was shown [11] that multistep cascading can be achieved by two second-order nonlinear cascading processes, SHG and sum-frequency mixing (SFM), and these two processes can also support a novel class of multi-colour parametric solitons [12], briefly discussed below.

B. Multistep cascading solitons

To introduce the simplest model of multistep cascading, we consider the fundamental beam with frequency ω entering a noncentrosymmetric nonlinear medium with a quadratic response. As a first step, the second-harmonic wave with frequency 2ω is generated via the SHG process. As a second step, we expect the generation of higher order harmonics due to SFM, for example, a third harmonic ($\omega + 2\omega = 3\omega$) or even fourth harmonic ($2\omega + 2\omega = 4\omega$) [13]. When both such processes are nearly phase matched, they can lead, via down-conversion, to a large nonlinear phase shift of the fundamental wave [11]. Additionally, the multistep cascading can support *a novel type of three-wave spatial solitary waves* in a diffractive $\chi^{(2)}$ nonlinear medium, *multistep cascading solitons*.

We start our analysis with the reduced amplitude equations derived in the slowly varying envelope approximation with the assumption of zero absorption of all interacting waves (see, e.g., Ref. [11]). Introducing the effect of diffraction in a slab waveguide geometry, we obtain

$$2ik_1\frac{\partial A_1}{\partial z} + \frac{\partial^2 A_1}{\partial x^2} + \chi_1 A_3 A_2^* e^{-i\Delta k_3 z}$$
$$+ \chi_2 A_2 A_1^* e^{-i\Delta k_2 z} = 0,$$

$$4ik_1\frac{\partial A_2}{\partial z} + \frac{\partial^2 A_2}{\partial x^2} + \chi_4 A_3 A_1^* e^{-i\Delta k_3 z} \qquad (5)$$
$$+ \chi_5 A_1^2 e^{i\Delta k_2 z} = 0,$$

$$6ik_1\frac{\partial A_3}{\partial z} + \frac{\partial^2 A_3}{\partial x^2} + \chi_3 A_2 A_1 e^{i\Delta k_3 z} = 0,$$

where $\chi_{1,2} = 2k_1\sigma_{1,2}$, $\chi_3 = 6k_1\sigma_3$, and $\chi_{4,5} = 4k_1\sigma_{4,5}$, and the nonlinear coupling coefficients σ_k are proportional to the elements of the second-order susceptibility tensor which we assume to satisfy the following relations (no dispersion), $\sigma_3 = 3\sigma_1$, $\sigma_2 = \sigma_5$, and $\sigma_4 = 2\sigma_1$.

In Eqs. (5), A_1, A_2 and A_3 are the complex electric field envelopes of the fundamental harmonic (FH), second

harmonic (SH), and third harmonic (TH), respectively, $\Delta k_2 = 2k_1 - k_2$ is the wavevector mismatch for the SHG process, and $\Delta k_3 = k_1 + k_2 - k_3$ is the wavevector mismatch for the SFM process. The subscripts '1' denote the FH wave, the subscripts '2' denote the SH wave, and the subscripts '3', the TH wave. Following the technique earlier employed in Refs. [14], we look for stationary solutions of Eq. (5) and introduce the normalised envelope $w(z, x)$, $v(z, x)$, and $u(z, x)$ according to the relations,

$$
\begin{aligned}
A_1 &= \frac{\sqrt{2}\beta k_1}{\sqrt{\chi_2 \chi_5}} e^{i\beta z} w, \\
A_2 &= \frac{2\beta k_1}{\chi_2} e^{2i\beta z + i\Delta k_2 z} v, \\
A_3 &= \frac{\sqrt{2\chi_2}\beta k_1}{\chi_1 \sqrt{\chi_5}} e^{3i\beta z + i\Delta k z} u,
\end{aligned}
\tag{6}
$$

where $\Delta k \equiv \Delta k_2 + \Delta k_3$. Renormalising the variables as $z \to z/\beta$ and $x \to x/\sqrt{2\beta k_1}$, we finally obtain a system of coupled equations,

$$
\begin{aligned}
i\frac{\partial w}{\partial z} + \frac{\partial^2 w}{\partial x^2} - w + w^* v + v^* u &= 0, \\
2i\frac{\partial v}{\partial z} + \frac{\partial^2 v}{\partial x^2} - \alpha v + \frac{1}{2} w^2 + w^* u &= 0, \\
3i\frac{\partial u}{\partial z} + \frac{\partial^2 u}{\partial x^2} - \alpha_1 u + \chi v w &= 0,
\end{aligned}
\tag{7}
$$

where $\alpha = 2(2\beta + \Delta k_2)/\beta$ and $\alpha_1 = 3(3\beta + \Delta k)/\beta$ are two dimensionless parameters that characterise the nonlinear phase matching between the parametrically interacting waves. Dimensionless material parameter $\chi \equiv \chi_1 \chi_3 / \chi_2^2 = 9(\sigma_1/\sigma_2)^2$ depends on the type of phase matching, and it can take different values of order of one. For example, when both SHG and SFM are due to quasi-phase matching (QPM), we have $\sigma_j = (2/\pi m)(\pi/\lambda_1 n_1)\chi^{(2)}[\omega; (4-j)\omega; -(3-j)\omega]$, where $j = 1, 2$. Then, for the first-order ($m = 1$) QPM processes (see, e.g., Ref. [15]), we have $\sigma_1 = \sigma_2$, and therefore $\chi = 9$. When SFM is due to the third-order QPM process (see, e.g., Ref. [16]), we should take $\sigma_1 = \sigma_2/3$, and therefore $\chi = 1$. At last, when SFM is the fifth-order QPM process, we have $\sigma_1 = \sigma_2/5$ and $\chi = 9/25$.

Dimensionless equations (7) present a fundamental model for three-wave multistep cascading solitons in the absence of walk-off. Additionally to the type I SHG solitons (see, e.g., Refs [14]), the multistep cascading solitons involve the phase-matched SFM interaction ($\omega + 2\omega = 3\omega$) that generates a third harmonic wave. Two-parameter family of localised solutions consists of three mutually coupled waves. It is interesting to note that, similar to the case of nondegenerate three-wave mixing [17], Eqs. (7) possess an exact solution. To find it, we make a substitution $w = w_0 \operatorname{sech}^2(\eta x)$, $v = v_0 \operatorname{sech}^2(\eta x)$ and $u = u_0 \operatorname{sech}^2(\eta x)$, and obtain unknown parameters from the following algebraic equations

$$
w_0^2 = \frac{9v_0}{3 + 4\chi v_0}, \quad 4\chi v_0^2 + 6v_0 = 9, \quad u_0 = \frac{2}{3}\chi w_0 v_0, \tag{8}
$$

valid for $\eta = \frac{1}{2}$ and $\alpha = \alpha_1 = 1$. Equations (8) have two solutions corresponding to *positive* and *negative* values of the amplitude (w_0). This indicates a possibility of multi-valued solutions, even within the class of exact solutions.
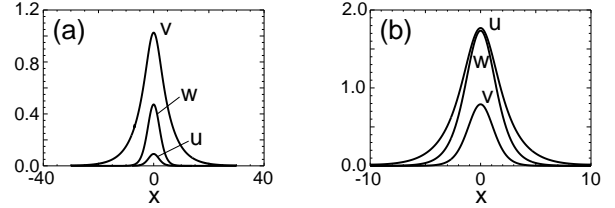
FIG. 3.   Examples of three-wave solitary waves of the model (7) for (a) $\alpha = 0.05$, $\alpha_1 = 5$, and (b) $\alpha = 5$, $\alpha_1 = 0.35$.

In general, three-wave solitons of Eqs. (7) can be found only numerically. Figures 3(a) and 3(b) present two examples of solitary waves for different sets of the mismatch parameters α and α_1. When $\alpha_1 \gg 1$ [see Fig. 3(a)], which corresponds to an unmatched SFM process, the amplitude of the third harmonic is small, and it vanishes for $\alpha_1 \to \infty$.
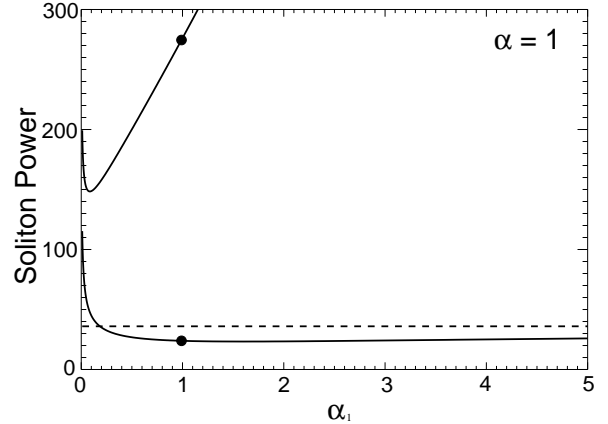
FIG. 4.   Two branches of multistep cascading solitons shown as the total soliton power P vs. the parameter α_1 for $\alpha = 1$ and $\chi = 1$. Filled circles show the analytical solutions. The lower branch approaches a family of two-wave quadratic solitons (for $\alpha_1 \to \infty$) shown by a dashed line.

To summarise different types of three-wave solitary waves, in Fig. 4 we plot the dependence of the total soliton power defined as

$$
P = \int_{-\infty}^{+\infty} dx \left(|w|^2 + 4|v|^2 + \frac{9}{\chi}|u|^2 \right), \tag{9}
$$

on the mismatch parameter α_1, for fixed $\alpha = 1$. It is clearly seen that for some values of α_1 (including the exact solution at $\alpha_1 = 1$ shown by two filled circles), there

exist *two different branches* of three-wave solitary waves, and only one of those branches approaches, for large values of α_1, a family of two-wave solitons of the cascading limit (Fig. 4, dashed). The slope of the branches changes from negative (for small α_1) to positive (for large α_1), indicating a possible change of the soliton stability. However, the detailed analysis of the soliton stability is beyond the scope of this paper (see, e.g., Refs. [18,19]).

C. Parametric soliton-induced waveguides

Another type of multistep cascading parametric processes which involve only two frequencies, i.e. *two-colour multistep cascading*, can occur due to the vectorial interaction of waves with different polarization. We denote two orthogonal polarization components of the fundamental harmonic (FH) wave ($\omega_1 = \omega$) as A and B, and two orthogonal polarizations of the second harmonic (SH) wave ($\omega_2 = 2\omega$), as S and T. Then, a simple multistep cascading process consists of the following steps. First, the FH wave A generates the SH wave S via type I SHG process. Then, by down-conversion SA-B, the orthogonal FH wave B is generated. At last, the initial FH wave A is reconstructed by the processes SB-A or AB-S, SA-A. Two principal second-order processes AA-S and AB-S correspond to *two different components* of the $\chi^{(2)}$ susceptibility tensor, thus introducing additional degrees of freedom into the parametric interaction. Different cases of such type of multistep cascading processes are summarized in Table I.

TABLE I. Two-frequency multistep cascading processes

	Principal	Equivalent
(a)	(AA-S, AB-S)	(BB-S, AB-S); (AA-T, AB-T) (BB-T, AB-T)
(b)	(AA-S, AB-T)	(BB-S, AB-T); (AA-T, AB-S) (BB-T, AB-S)
(c)	(AA-S, BB-S)	(AA-T, BB-T)
(d)	(AA-S, AA-T)	(BB-S, BB-T)

To demonstrate some of the unique properties of the multistep cascading, we discuss here how it can be employed for soliton-induced waveguiding effects in quadratic media. For this purpose, we consider a model of two-frequency multistep cascading described by the principal DPM process (c) (see Table I above) in the planar slab-waveguide geometry. Using the slowly varying envelope approximation with the assumption of zero absorption of all interacting waves, we obtain

$$2ik_1\frac{\partial A}{\partial z} + \frac{\partial^2 A}{\partial x^2} + \chi_1 SA^* e^{-i\Delta k_1 z} = 0,$$

$$2ik_1\frac{\partial B}{\partial z} + \frac{\partial^2 B}{\partial x^2} + \chi_2 SB^* e^{-i\Delta k_2 z} = 0, \qquad (10)$$

$$4ik_1\frac{\partial S}{\partial z} + \frac{\partial^2 S}{\partial x^2} + 2\chi_1 A^2 e^{i\Delta k_1 z} + 2\chi_2 B^2 e^{i\Delta k_2 z} = 0,$$

where $\chi_{1,2} = 2k_1\sigma_{1,2}$, the nonlinear coupling coefficients σ_k are proportional to the elements of the second-order susceptibility tensor, and Δk_1 and Δk_2 are the corresponding wave-vector mismatch parameters.

To simplify the system (10), we look for its stationary solutions and introduce the normalized envelopes u, v, and w according to the following relations, $A = \gamma_1 u \exp(i\beta z - \frac{i}{2}\Delta k_1 z)$, $B = \gamma_2 v \exp(i\beta z - \frac{i}{2}\Delta k_2 z)$, and $S = \gamma_3 w \exp(2i\beta z)$, where $\gamma_1^{-1} = 2\chi_1 x_0^2$, $\gamma_2^{-1} = 2x_0^2(\chi_1\chi_2)^{1/2}$, and $\gamma_3^{-1} = \chi_1 x_0^2$, and the longitudinal and transverse coordinates are measured in the units of $z_0 = (\beta - \Delta k_1/2)^{-1}$ and $x_0 = (z_0/2k_1)^{1/2}$, respectively. Then, we obtain a system of normalized equations,

$$i\frac{\partial u}{\partial z} + \frac{\partial^2 u}{\partial x^2} - u + u^* w = 0,$$

$$i\frac{\partial v}{\partial z} + \frac{\partial^2 v}{\partial x^2} - \alpha_1 v + \chi v^* w = 0, \qquad (11)$$

$$2i\frac{\partial w}{\partial z} + \frac{\partial^2 w}{\partial x^2} - \alpha w + \frac{1}{2}(u^2 + v^2) = 0,$$

where $\chi = (\chi_2/\chi_1)$, $\alpha_1 = (\beta - \Delta k_2/2)(\beta - \Delta k_1/2)^{-1}$, and $\alpha = 4\beta\,(\beta - \Delta k_1/2)^{-1}$.

First of all, we notice that for $v = 0$ (or, similarly, $u = 0$), the dimensionless Eqs. (11) reduce to the corresponding model for the two-step cascading due to type I SHG discussed earlier [3,4], and its stationary solutions are defined by the equations for real u and w,

$$\frac{d^2 u}{dx^2} - u + uw = 0,$$

$$\frac{d^2 w}{dx^2} - \alpha w + \frac{1}{2}u^2 = 0, \qquad (12)$$

that possess a one-parameter family of two-wave localized solutions (u_0, w_0) found earlier numerically for any $\alpha \neq 1$, and also known analytically for $\alpha = 1$, $u_0(x) = (3/\sqrt{2})\mathrm{sech}^2(x/2) = \sqrt{2}w_0(x)$ (see Ref. [4]).

Then, in the small-amplitude approximation, the equation for real orthogonally polarized FH wave v can be treated as an eigenvalue problem for an effective waveguide created by the SH field $w_0(x)$,

$$\frac{d^2 v}{dx^2} + [\chi\,w_0(x) - \alpha_1]v = 0. \qquad (13)$$

Therefore, an additional parametric process allows to propagate a probe beam of one polarization in *an effective waveguide* created by a two-wave spatial soliton in a quadratic medium with FH component of another polarization. However, this type of waveguide is different from what has been studied for Kerr-like solitons because it is *coupled parametrically* to the guided modes and, as a result, the physical picture of the guided modes is valid, rigorously speaking, only in the case of stationary phase-matched beams. As a result, the stability of the corresponding waveguide and localized modes of the orthogonal polarization it guides is a key issue. In particular,

6

the waveguide itself (i.e. *two-wave parametric soliton*) becomes unstable for $\alpha < \alpha_{cr} \approx 0.2$ [18].

In order to find the guided modes of the parametric waveguide created by a two-wave quadratic soliton, we have to solve Eq. (13) where the exact solution $w_0(x)$ is to be found numerically. Then, to address this problem analytically, approximate solutions can be used, such as those found with the help of the variational method [20]. However, the different types of the variational ansatz used do not provide a very good approximation for the soliton profile at all α. For our eigenvalue problem (13), the function $w_0(x)$ defines parameters of the guided modes and, in order to obtain accurate results, it should be calculated as close as possible to the exact solutions found numerically. To resolve this difficulty, below we suggest a novel "almost exact" solution that *would allow to solve analytically many of the problems involving quadratic solitons*, including the eigenvalue problem (13).

First, we notice that from the exact solution at $\alpha = 1$ and the asymptotic result for large α, $w \approx u^2/(2\alpha) \approx 2\,\mathrm{sech}^2(x)$, it follows that the SH component $w_0(x)$ of Eqs. (12) remains almost self-similar for $\alpha \geq 1$. Thus, we look for the SH field in the form $w_0(x) = w_m\,\mathrm{sech}^2(x/p)$, where w_m and p are to be defined. The solution for $u_0(x)$ should be consistent with this choice of the shape for SH, and it is defined by the first (linear for u) equation of the system (12). Therefore, we can take u in the form of the lowest guided mode, $u_0(x) = u_m\,\mathrm{sech}^p(x/p)$, that corresponds to an effective waveguide $w_0(x)$. By matching the asymptotics of these trial functions with those defined directly from Eqs. (12) at small and large x, we obtain the following solution,

$$u_0(x) = u_m \mathrm{sech}^p(x/p), \quad w_0(x) = w_m \mathrm{sech}^2(x/p), \quad (14)$$

$$u_m^2 = \frac{\alpha w_m^2}{(w_m - 1)}, \; p = \frac{1}{(w_m - 1)}, \; \alpha = \frac{4(w_m - 1)^3}{(2 - w_m)}. \quad (15)$$

Here, the third relation allows us to find w_m for arbitrary α as a solution of a cubic equation, and then to find all other parameters as functions of α. For mismatches in the interval $0 < \alpha < +\infty$, the parameter values change monotonically in the regions: $0 < u_m < +\infty$, $1 < w_m < 2$, and $+\infty > p > 1$. It is really amazing that the analytical solution (14),(15) provides *an excellent approximation* for the profiles of the two-wave parametric solitons found numerically, with the relative errors not exceeding 1%–3% for stable solitons (e.g. when $\alpha > \alpha_{cr}$). As a matter of fact, we can treat Eqs. (14) and (15) as an *approximate scaling transformation* of the family of two-wave bright solitons. Moreover, this solution allows us to capture some remarkable internal similarities and distinctions between the solitons existing in different types of nonlinear media. In particular, as follows from Eqs. (14) and (15), the FH component and the self-consistent effective waveguide (created by the SH field) have approximately the same stationary transverse profiles as for one-component solitons in a Kerr-like medium with power-law nonlinear response [21]. For $\alpha = 1$ ($p = 2$) and $\alpha \gg 1$

($p = 1$) our general expressions reduce to the known analytical solutions, and the FH profile is exactly the same as that for solitons in quadratic and cubic Kerr media, respectively. On the other hand, the strength of self-action for quadratic solitons depends on the normalized phase mismatch α and, in general, the beam dynamics for parametric wave mixing can be very different from that observed in Kerr-type media.

Now, the eigenvalue problem (13) can be readily solved analytically. The eigenmode cutoff values are defined by the parameter α_1 that takes one of the discrete values, $\alpha_1^{(n)} = (s - n)^2/p^2$, where $s = -(1/2) + [(1/4) + w_m \chi p^2]^{1/2}$. Number n stands for the mode order ($n = 0, 1, \ldots$), and the localized solutions are possible provided $n < s$. The profiles of the corresponding guided modes are

$$v_n(x) = V \mathrm{sech}^{s-n}(x/p) H(-n, 2s - n + 1, s - n + 1; \zeta/2),$$

where $\zeta = 1 - \tanh(x/p)$, H is the hypergeometric function, and V is the mode's amplitude which cannot be determined within the framework of the linear analysis.
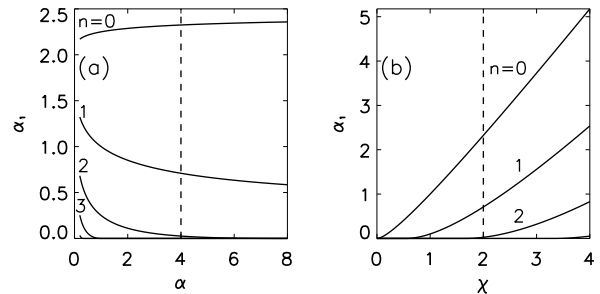

FIG. 5. Cutoff eigenvalues $\alpha_1^{(n)}$ of the guided modes shown as (a) functions of α at $\chi = 2$, and (b) functions of χ at $\alpha = 4$. Dashed lines correspond to the intersection of the plots in the parameter space (α, χ).

According to these results, a two-wave parametric soliton creates, a multi-mode waveguide and larger number of the guided modes can be observed for smaller α. Figures 5(a,b) show the dependence of the mode cutoff values $\alpha_1^{(n)}(\alpha)$ for a fixed χ, and $\alpha_1^{(n)}(\chi)$ for a fixed α, respectively. For the case $\chi = 1$, the dependence has a simple form: $\alpha_1^{(n)}(\alpha) = [1 - n(w_m - 1)]^2$.

Because a two-wave soliton creates an induced waveguide parametrically coupled to its guided modes of the orthogonal polarization, the dynamics of the guided modes *may differ drastically* from that of conventional waveguides based on the Kerr-type nonlinearities. Figures 6(a-d) show two examples of the evolution of guided modes. In the first example [see Fig. 6(a-c)], a weak fundamental mode is amplified via parametric interaction with a soliton waveguide, and the mode experiences a strong power exchange with the orthogonally polarized

FH component through the SH field. This process is accompanied by only a weak deformation of the induced waveguide [see Fig. 6(a) – dotted curve]. The resulting effect can be interpreted as a power exchange between two guided modes of orthogonal polarizations in a waveguide created by the SH field. In the second example, the propagation is stable [see Fig. 6(d)].

When all the fields in Eq. (11) are not small, i.e. the small-amplitude approximation is no longer valid, the profiles of the three-component solitons should be found numerically. However, some of the lowest-order states can be calculated approximately using the approach of the "almost exact" solution (14),(15) described above, which is presented in detail elsewhere [22,23]. Moreover, a number of the solutions and their families can be obtained in *an explicit analytical form*. For example, for $\alpha_1 = 1/4$, there exist two *families of three-component solitary waves* for any $\alpha \geq 1$, that describe soliton branches starting at the bifurcation points $\alpha_1 = \alpha_1^{(1)}$ at $\alpha = 1$: (i) the soliton with a zero-order guided mode for $\chi = 1/3$: $u(x) = \left(3/\sqrt{2}\right)\operatorname{sech}^2(x/2)$, $v(x) = c_2 \operatorname{sech}(x/2)$, $w(x) = (3/2)\operatorname{sech}^2(x/2)$, and (ii) the soliton with a first-order guided mode for $\chi = 1$: $u(x) = c_1 \operatorname{sech}^2(x/2)$, $v(x) = c_2 \operatorname{sech}^2(x/2)\sinh(x/2)$, $w(x) = (3/2)\operatorname{sech}^2(x/2)$, where $c_2 = \sqrt{3(\alpha-1)}$ and $c_1 = \sqrt{(9/2)+c_2^2}$.
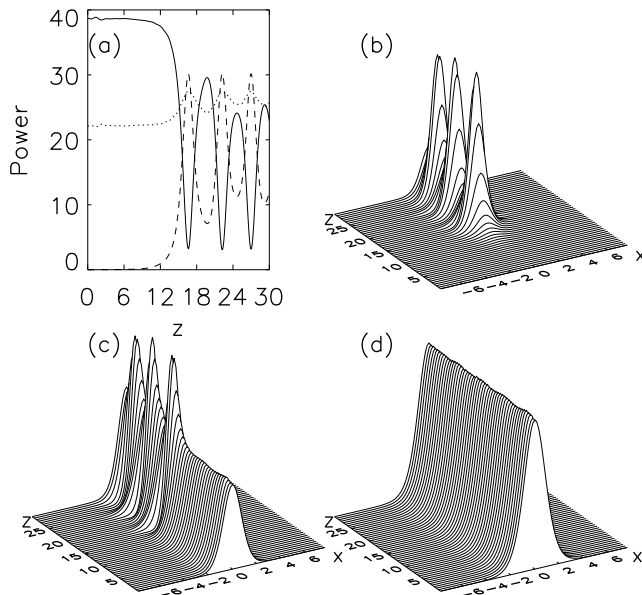

FIG. 6. (a) Change of the normalized power in FH (u, solid) and SH (w, dotted) components, which initially constitute a two-wave soliton, and in the guided mode (v, dashed) at $\chi = 2$, demonstrating amplification of a guided wave. Evolution of the guided wave and effective waveguide (SH) is presented in plots (b) and (c), respectively. (d) Stationary propagation of a stable fundamental mode ($\chi = 1$). For all the plots $\alpha = 4$, the initial amplitude is $v_0 = 0.1$, and α_1 corresponds to the bifurcation point.

For a practical realization of the DPM processes and the soliton waveguiding effects described above, we can suggest two general methods. The first method is based on the use of *two commensurable periods* of the quasi-phase-matched (QPM) periodic grating. Indeed, to achieve DPM, we can employ the first-order QPM for one parametric process, and the third-order QPM, for the other parametric process. Taking, as an example, the parameters for LiNbO$_3$ and AA-S ($xx - z$) and BB-S ($zz - z$) processes [24], we find two points for DPM at about 0.89 μm and 1.25 μm. This means that a single QPM grating can provide simultaneous phase-matching for two parametric processes. For such a configuration, we obtain $\chi \approx 1.92$ or, interchanging the polarization components, $\chi \approx 0.52$. The second method to achieve the conditions of DPM processes is based on the idea of *quasi-periodic QPM grating* [25,26]. Specifically, Fibonacci optical superlattices provide an effective way to achieve phase-matching at *several incommensurable periods* allowing multi-frequency harmonic generation in a single structure. We describe the properties of such structures in the next section.

V. ENVELOPE SOLITONS IN FIBONACCI SUPERLATTICES

A. Incoherence and solitary waves

For many years, solitary waves have been considered as *coherent localized modes* of nonlinear systems, with particle-like dynamics quite dissimilar to the irregular and stochastic behavior observed for chaotic systems [27]. However, about 20 years ago Akira Hasegawa, while developing a statistical description of the dynamics of an ensemble of plane waves in nonlinear strongly dispersive plasmas, suggested the concept of a localized envelope of random phase waves [28]. Because of the relatively high powers required for generating self-localized random waves, this notion remained a theoretical curiosity until recently, when the possibility to generate spatial optical solitons by a partially incoherent source was discovered in a photorefractive medium [29].

The concept of incoherent solitons can be compared with a different problem: the propagation of a soliton through a spatially disordered medium. Indeed, due to random scattering on defects, the phases of the individual components forming a soliton experience random fluctuations, and the soliton itself becomes *partially incoherent* in space and time. For a low-amplitude wave (linear regime) spatial incoherence is known to lead to a fast decay. As a result, the transmission coefficient vanishes exponentially with the length of the system, the phenomenon known as Anderson localization [30]. However, for large amplitudes (nonlinear regime), when the nonlinearity length is much smaller than the Anderson localization length, a soliton can propagate almost unchanged

through a disordered medium as predicted theoretically in 1990 [31] and recently verified experimentally [32].

These two important physical concepts, spatial self-trapping of light generated by an incoherent source in a homogeneous medium, and suppression of Anderson localization for large-amplitude waves in spatially disordered media, both result from the effect of strong nonlinearity. When the nonlinearity is sufficiently strong it acts as *an effective phase-locking mechanism* by producing a large frequency shift of the different random-phase components, and thereby introducing *an effective order* into an incoherent wave packet, thus enabling the formation of localized structures. In other words, both phenomena correspond to the limit when the ratio of the nonlinearity length to the characteristic length of (spatial or temporal) fluctuations is small. In the opposite limit, when this ratio is large, the wave propagation is practically linear.

Below we show that, at least for aperiodic inhomogeneous structures, solitary waves can exist in the intermediate regime in the form of *quasiperiodic nonlinear localized modes.* As an example, we consider SHG and nonlinear beam propagation in *Fibonacci optical superlattices*, and demonstrate numerically the possibility of spatial self-trapping of quasiperiodic waves whose envelope amplitude varies quasiperiodically, while still maintaining a stable, well-defined spatially localized structure, *a quasiperiodic envelope soliton.*

B. Quasi-phase-matching in optical superlattices

We consider the interaction of a fundamental wave with the frequency ω (FH) and its SH in a slab waveguide with quadratic (or $\chi^{(2)}$) nonlinearity. Assuming the $\chi^{(2)}$ susceptibility to be modulated and the nonlinearity to be of the same order as diffraction, we write the dynamical equations in the form

$$
\begin{aligned}
&i\frac{\partial u}{\partial z} + \frac{1}{2}\frac{\partial^2 u}{\partial x^2} + d(z)u^* v e^{-i\beta z} = 0, \\
&i\frac{\partial w}{\partial z} + \frac{1}{4}\frac{\partial^2 w}{\partial x^2} + d(z)u^2 e^{i\beta z} = 0,
\end{aligned}
\tag{16}
$$

where $u(x, z)$ and $w(x, z)$ are the slowly varying envelopes of the FH and SH, respectively. The parameter $\beta = \Delta k |k_\omega| x_0^2$ is proportional to the phase mismatch $\Delta k = 2k_\omega - k_{2\omega}$, k_ω and $k_{2\omega}$ being the wave numbers at the two frequencies. The transverse coordinate x is measured in units of the input beam width x_0, and the propagation distance z in units of the diffraction length $l_d = x_0^2 |k_\omega|$. The spatial modulation of the $\chi^{(2)}$ susceptibility is described by the quasi-phase-matching (QPM) grating function $d(z)$. In the context of SHG, the QPM technique is an effective way to achieve phase matching, and it has been studied intensively [33].
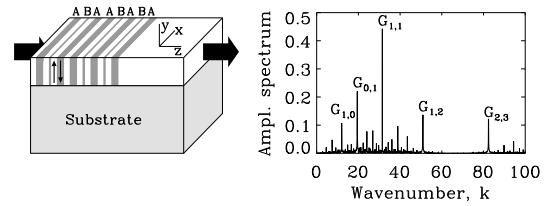

FIG. 7. (a) Slab waveguide with quasiperiodic QPM superlattice structure composed of building blocks A and B. (b) Numerically calculated amplitude spectrum of $d(z)$.

Here we consider a QPM grating produced by a quasiperiodic nonlinear optical superlattice. Quasiperiodic optical superlattices, one-dimensional analogs of quasicrystals [34], are usually designed to study the effect of Anderson localization in the linear regime of light propagation. For example, Gellermann *et al.* measured the optical transmission properties of quasiperiodic dielectric multilayer stacks of SiO_2 and TiO_2 thin films and observed a strong suppression of the transmission [35]. For QPM gratings, a nonlinear quasiperiodic superlattice of $LiTaO_3$, in which two antiparallel ferro-electric domains are arranged in a Fibonacci sequence, was recently fabricated by Zhu *et al.* [25], who measured multi-colour SHG with energy conversion efficiencies of $\sim 5\% - 20\%$. This quasiperiodic optical superlattice in $LiTaO_3$ can also be used for efficient direct third harmonic generation [26].

The quasiperiodic QPM gratings have two building blocks A and B of the length l_A and l_B, respectively, which are ordered in a Fibonacci sequence [Fig. 7(a)]. Each block has a domain of length $l_{A_1}=l$ ($l_{B_1}=l$) with $d=+1$ (shaded) and a domain of length $l_{A_2}=l(1 + \eta)$ [$l_{B_2}=l(1 - \tau\eta)$] with $d=-1$ (white). In the case of $\chi^{(2)}$ nonlinear QPM superlattices this corresponds to positive and negative ferro-electric domains, respectively. The specific details of this type of Fibonacci optical superlattices can be found elsewhere [25]. For our simulations presented below we have chosen $\eta= 2(\tau - 1)/(1 + \tau^2)=$ 0.34, where $\tau= (1 + \sqrt{5})/2$ is the so-called *golden ratio*. This means that the ratio of length scales is also the golden ratio, $l_A/l_B= \tau$. Furthermore, we have chosen $l=0.1$.

The grating function $d(z)$, which varies between $+1$ and -1 according to the Fibonacci sequence, can be expanded in a Fourier series

$$
d(z) = \sum_{m,n} d_{m,n} e^{iG_{m,n}z}, \quad G_{m,n} = \frac{2\pi(m + n\tau)}{D},
\tag{17}
$$

where $D=\tau l_A + l_B=0.52$ for the chosen parameter values. Hence the spectrum is composed of sums and differences of the basic wavenumbers $\kappa_1=2\pi/D$ and $\kappa_2=2\pi\tau/D$. These components fill the whole Fourier space densely, since κ_1 and κ_2 are incommensurate. Figure 7(b) shows the numerically calculated Fourier spectrum $G_{m,n}$. The lowest-order "Fibonacci modes" are clearly the most intense.

9

C. Quasiperiodic optical solitons

To analyze the beam propagation and SHG in a quasiperiodic QPM grating one could simply average Eqs. (16). To lowest order this approach always yields a system of equations with constant mean-value coefficients, which does not allow to describe oscillations of the beam amplitude and phase. However, here we wish to go beyond the averaged equations and consider the rapid large-amplitude variations of the envelope functions. This can be done analytically for periodic QPM gratings [36]. However, for the quasiperiodic gratings we have to resolve to numerical simulations.

Thus we have solved Eqs. (16) numerically with a second-order split-step routine. At the input of the crystal we excite the fundamental beam (corresponding to unseeded SHG) with a Gaussian profile,

$$u(x,0) = A_u \, e^{-x^2/10}, \quad w(x,0) = 0. \qquad (18)$$

We consider the quasiperiodic QPM grating with matching to the peak at $G_{2,3}$, i.e., $\beta = G_{2,3} = 82.25$. First, we study the small-amplitude limit when a weak FH is injected with a low amplitude. Figures 8(a,b) show an example of the evolution of FH and SH in this effectively linear regime. As is clearly seem from Fig. 8(b) the SH wave is excited, but both beams eventually diffract.

When the amplitude of the input beam exceeds a certain threshold, self-focusing and localization should be observed for both harmonics. Figures 8(c,d) show an example of the evolution of a strong input FH beam, and its corresponding SH. Again the SH is generated, but now the nonlinearity is so strong that it leads to self-focusing and mutual self-trapping of the two fields, resulting in a spatially localized two-component soliton, despite the continuous scattering of the quasiperiodic QPM grating.
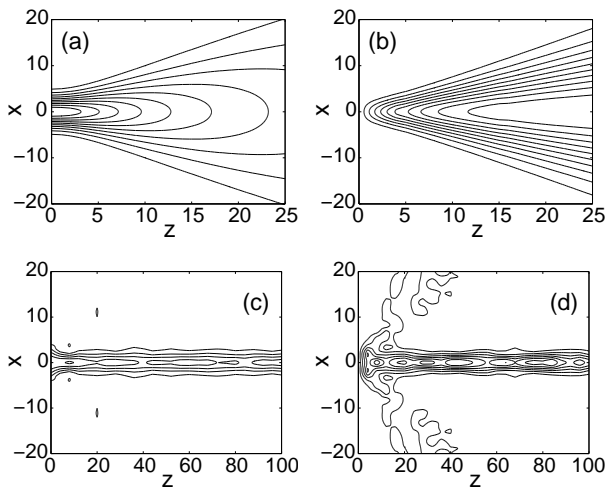

FIG. 8. (a) Diffraction of a weak FH beam with amplitude $A_u = 0.25$ for $\beta = 82.25$. (c) Excitation of a quasiperiodic soliton by a FH beam with amplitude $A_u = 5$ for $\beta = 82.25$. (b,d) Corresponding SH components.

It is important to notice that the two-component localized beam created due to the self-trapping effect is quasiperiodic by itself. As a matter of fact, after an initial transient its amplitude oscillates in phase with the quasiperiodic QPM modulation $d(z)$. This is illustrated in Fig. 9, where we show in more detail the peak intensities in the asymptotic regime of the evolution. The oscillations shown in Fig. 9 are in phase with the oscillations of the QPM grating $d(z)$, and we indeed found that their spectra are similar.
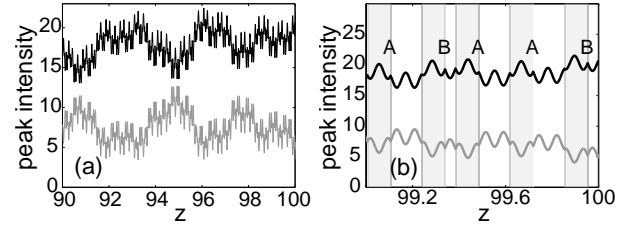

FIG. 9. Amplitude oscillations of the quasiperiodic soliton. (a),(b) Close-ups of the peak intensity $|u(0,z)|^2$ of the FH (black) and $|w(0,z)|^2$ of the SH (grey). The Fibonacci building blocks A and B are indicated in (b) with $d=1$ in grey regions, and $d=-1$ in white regions.

Our numerical results show that the quasiperiodic envelope solitons can be generated for a broad range of the phase-mismatch β. The amplitude and width of the solitons depend on the effective mismatch, which is the separation between β and the nearest strong peak $G_{m,n}$ in the Fibonacci QPM grating spectrum [see Fig. 7(b)]. Thus, low-amplitude broad solitons are excited for β-values in between peaks, whereas high-amplitude narrow solitons are excited when β is close to a strong peak, as shown in Fig. 8(c,d).
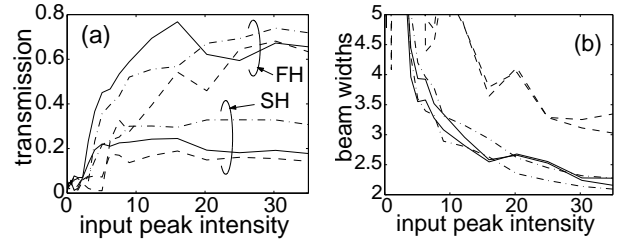

FIG. 10. (a) Transmission of the FH, $|u(0,L)/u(0,0)|^2$, and the SH, $|w(0,L)/u(0,0)|^2$ vs. input peak intensity $|u(0,0)|^2$ of the FH. (b) Output beam width vs. $|u(0,0)|^2$. $L=100$, $\beta = G_{1,2} = 50.83$ (solid), $\beta = G_{2,4} = 101.66$ (dashed), and $\beta = G_{2,3} = 82.25$ (dot-dashed).

To analyse in more detail the transition between the linear (diffraction) and nonlinear (self-trapping) regimes, we have made a series of careful numerical simulations [37]. In Fig. 10 we show the transmission coefficients and the beam widths at the output of the crystal versus the intensity of the FH input beam, for a variety of β-values. These dependencies clearly illustrate the

10

universality of the generation of localised modes for varying strength of nonlinearity, i.e. a quasiperiodic soliton is generated only for sufficiently high amplitudes. This is of course a general phenomenon also observed in many nonlinear isotropic media. However, here the self-trapping occurs for quasiperiodic waves, with the quasiperiodicity being preserved in the variation of the amplitude of both components of the soliton.

VI. CONCLUSION

We have overviewed several important physical examples of the multi-component solitary waves which appear due to multi-mode and/or multi-frequency coupling in nonlinear optical fibers and waveguides. We have described several types of such multi-component solitary waves, including: (i) multi-wavelength solitary waves in multi-channel bit-parallel-wavelength fiber transmission systems, (ii) multi-colour parametric spatial solitary waves due to multistep cascading in quadratic materials, and (iii) quasiperiodic envelope solitons in Fibonacci optical superlattices. These examples reveal some general features and properties of multi-component solitary waves in nonintegrable nonlinear models, also serving as a stepping stone for approaching other problems of the multi-mode soliton coupling and interaction.

ACKNOWLEDGMENTS

[1] A. Hasegawa and Y. Kodama, *Solitons in Optical Communications* (Clarendon Press, Oxford, 1995).
[2] L. A. Bergman, A. J. Mendez, and L. S. Lome, SPIE Crit. Rev. **CR 62**, 210 (1996).
[3] For a comprehensive overview of cascading, see G. Stegeman, D. J. Hagan, and L. Torner, Opt. Quantum Electron. **28**, 1691 (1996).
[4] For an overview of quadratic spatial solitons, see L. Torner, in: *Beam Shaping and Control with Nonlinear Optics*, F. Kajzer and R. Reinisch, Eds. (Plenum, New York, 1998), p. 229; Yu. S. Kivshar, In: *Advanced Photonics with Second-Order Optically Nonlinear Processes*, A. D. Boardman, L. Pavlov, and S. Tanev, Eds. (Kluwer, Dordretch, 1998), p. 451.
[5] C. Yeh and L. Bergman, J. Appl. Phys. **80**, 3174 (1996).
[6] G. P. Agrawal, *Nonlinear Fiber Optics* (Academic Press, New York, 1995), Sec. 7.1.
[7] C. Yeh and L. Bergman, Phys. Rev. E **60**, 2306 (1999).
[8] Yu. S. Kivshar and E. A. Ostrovskaya, LANL preprint: arXiv:patt-sol/9912008.
[9] C. R. Menyuk, J. Opt. Soc. Am. B **5**, 392 (1988); Yu. S. Kivshar, J. Opt. Soc. Am. B **7**, 2204 (1990).
[10] See, e.g, G. Assanto, I. Torelli, and S. Trillo, Opt. Lett. **19**, 1720 (1994); A. D. Boardman, P. Bontemps, and K. Xie, Opt. Quantum Electron. **30**, 891 (1998).
[11] K. Koynov and S. Saltiel, Opt. Commun. **152**, 96 (1998).
[12] Yu. S. Kivshar, T. J. Alexander, and S. Saltiel, Opt. Lett. **24**, 759 (1999).
[13] See, e.g., S. A. Akhmanov, A. N. Dubrovik, S. M. Saltiel, I. V. Tomov, and V. G. Tunkin, Pis'ma Zh. Éksp. Teor. Fiz. **20**, 264 (1974) [JETP Lett. **20**, 117 (1974)].
[14] A. V. Buryak and Yu. S. Kivshar, Opt. Lett. **20**, 1612 (1994); Phys. Lett. A **197**, 407 (1995).
[15] O. Pfister, J. S. Wells, L. Hollberg, L. Zink, D. A. Van Baak, M. D. Levenson, and W. R. Basenberg, Opt. Lett. **22**, 1211 (1997).
[16] P. Baldi, C. G. Treviño-Palacios, G. I. Stegeman, M. P. De Micheli, D. B. Ostrowsky, D. Delacourt, and M. Papuchon, Electron. Lett. **31**, 1350 (1995).
[17] B. A. Malomed, D. Anderson, and M. Lisak, Opt. Commun. **126**, 251 (1996).
[18] D. E. Pelinovsky, A. V. Buryak, and Yu. S. Kivshar, Phys. Rev. Lett. **75**, 591 (1995).
[19] A. V. Buryak, Yu. S. Kivshar, and S. Trillo, Phys. Rev. Lett. **77**, 5210 (1996).
[20] V. V. Steblina *et al.*, Opt. Commun. **118**, 345 (1995); A. D. Boardman *et al.*, Phys. Rev. A **52**, 4099 (1995); V. M. Agranovich *et al.*, Phys. Rev. B **53**, 15451 (1996).
[21] C. Sulem and P.-L. Sulem, *The Nonlinear Schrödinger Equation: Self-Focusing and Wave Collapse*, (Springer-Verlag, New York, 1999).
[22] A. A. Sukhorukov, Phys. Rev. E **61**, 4530 (2000).
[23] Yu. S. Kivshar, A. A. Sukhorukov, and S. M. Saltiel, Phys. Rev. E **60**, R5056 (1999).
[24] V. G. Dmitriev, G. G. Gurzadyan, and D. N. Nikogosyan, *Handbook of Nonlinear Optical Crystals* (Springer, Berlin, 1997).
[25] S. Zhu, Y. Zhu, Y. Qin, H. Wang, C. Ge, and N. Ming, Phys. Rev. Lett. **78**, 26752 (1997).
[26] S. Zhu, Y. Zhu, and N. Ming, Science **278**, 843 (1997); Y. Zhu *et al.*, Appl. Phys. Lett. **73**, 432 (1998).
[27] See, e.g., *Future Directions of Nonlinear Dynamics in Physical and Biological Systems*, P. L. Christiansen *et al.*, Eds., NATO ASI Series B: Physics, Vol. 312 (Plenum Press, New York, 1993).
[28] A. Hasegawa, Phys. Fluids **18**, 77 (1975); Phys. Fluids **20**, 2155 (1977).
[29] M. Mitchell *et al.*, Phys. Rev. Lett. **77**, 490 (1996); M. Mitchell and M. Segev, Nature **387**, 880 (1997); Z. Chen *et al.*, Science **280**, 889 (1998).
[30] See, e.g., S. A. Gredeskul and Yu. S. Kivshar, Phys. Rep. **216**, 1 (1992), and references therein.
[31] Yu. S. Kivshar, S. A. Gredeskul, A. Sánchez, and L. Vázquez, Phys. Rev. Lett. **64**, 1693 (1990).
[32] V. A. Hopkins, J. Keat, G. D. Meegan, T. Zhang, and J. D. Maynard, Phys. Rev. Lett. **76**, 1102 (1996).

[33] For a comprehensive overview of the QPM technique, see M. M. Fejer, G. A. Magel, D. H. Jundt, and R. L. Byer, IEEE J. Quantum Electron. **28**, 2631 (1992).

[34] D. Schechtman, I. Blech, D. Gratias, and J. W. Cahn, Phys. Rev. Lett. **53**, 1951 (1984).

[35] W. Gellermann, M. Kohmoto, B. Sutherland, and P. C. Taylor, Phys. Rev. Lett. **72**, 63 (1994).

[36] C. Balslev Clausen, O. Bang, and Yu. S. Kivshar, Phys. Rev. Lett. **78**, 4749 (1997).

[37] C. Balslev Clausen, Yu. S. Kivshar, O. Bang, and P. L. Christiansen, Phys. Rev. Lett. **83**, 4740 (1999).